frontiers in Earth Science

ORIGINAL RESEARCH
published: 20 January 2021
doi: 10.3389/feart.2020.633342

Using Google Earth Images to Extract Dense Landslides Induced by Historical Earthquakes at the Southwest of Ordos, China

Du Peng, Xu Yueren, Tian Qinjian and Li Wenqiao*

Key Laboratory of Earthquake Prediction, Institute of Earthquake Forecasting, China Earthquake Administration, Beijing, China

As historical earthquake records are simple, determining the source parameters of historical strong earthquakes over an extended period is difficult. There are numerous uncertainties in the study of historical earthquakes based on limited literature records. Co-seismic landslide interpretation combined with historical documents can yield the possibility of reducing these uncertainties. The dense co-seismic landslides can be preserved for hundreds to thousands of years in Loess Plateau, North China; furthermore, there are notable attribute differences between earthquake landslides and rainfall-triggered landslides. Along the southwestern margin of the Ordos Block, only one severe earthquake has been recorded in the past 3,000 years. The records of "Sanchuan exhaustion and Qishan collapse" provide clues for an investigation of the 780 BC Qishan earthquake. In this study, combined with historical documents, current high-resolution Google Earth images were used to extract historical landslides along the southwestern of the Ordos Block. There were 6,876 landslides with a total area of 643 km^2. The landslide-intensive areas were mainly distributed along the Longxian–Qishan–Mazhao Fault in the loess valley area on the northeastern side of the fault. Loess tableland and river terraces occur on the southwest side of the fault; dense landslides have not been examined due to the topographical conditions in this area. By analyzing the spatial distribution of historical earthquake damage in this region, comparing the characteristics of rainfall-triggered landslides, and combining existing dating results for bedrock collapse and loess landslides, the interpretation of dense historical landslides can be linked to the Qishan Earthquake. The interpretation results are associated with historical records. Analyses of current earthquake cases show that the distribution of dense landslides triggered by strong earthquakes can indicate the episeismic area of an earthquake. In addition, the non-integrated landslide catalog without small- and medium-scale coseismic landslides can be used to effectively determine the source parameters of historical strong earthquakes and perform quantitative evaluations. This study evaluates the focal parameters of the 780 BC Qishan earthquake based on interpretations of the spatial distribution range of historical landslides as representations of the range of the extreme earthquake zone.

Keywords: 780BC Qishan Earthquake, Earthquake-triggered landslides, Loess plateau, Google Earth, seismic parameters

OPEN ACCESS

Edited by:
Chong Xu,
National Institute of Natural Hazards, China

Reviewed by:
Jixiang Xu,
China University of Geosciences, China
Yulong Cui,
Anhui University of Science and Technology, China

****Correspondence:***
Xu Yueren
39021865@qq.com

Specialty section:
This article was submitted to Geohazards and Georisks, a section of the journal Frontiers in Earth Science

Received: *25 November 2020*
Accepted: *17 December 2020*
Published: *20 January 2021*

Citation:
Peng D, Yueren X, Qinjian T and Wenqiao L (2021) Using Google Earth Images to Extract Dense Landslides Induced by Historical Earthquakes at the Southwest of Ordos, China. Front. Earth Sci. 8:633342. doi: 10.3389/feart.2020.633342

INTRODUCTION

The macro-epicenter, magnitude, range of influence, and rupture scale of historical earthquakes are mostly based on damages recorded in historical documents. However, for earlier historical earthquakes, due to the long history and unknown or missing historical records, determining the relevant seismic parameters is often difficult, or there is significant uncertainty. Previous studies have shown that in addition to fault investigations, the spatial distribution of coseismic landslides can indicate the seismic intensity and rupture zone (Dadson et al., 2004; Meunier et al., 2008; Larsen et al., 2010; Parker et al., 2011; Yuan D et al., 2013). The Wenchuan earthquake produced a 240 km long surface rupture zone. Within the 240 km range, the cumulative number of landslides accounted for 86% of the total landslides triggered by the Wenchuan earthquake, and the cumulative landslide area accounted for 91% of the total landslides triggered by the Wenchuan earthquake. Landslides triggered by the Wenchuan earthquake were mainly distributed in the IX degree area. The landslide area within the IX degree area accounted for 81.1% of the total landslide area while the landslide number accounted for 76.6% of the total landslide number (Du et al., 2020a). The distribution of 5,019 landslides triggered by the Tongwei earthquake in 1718 coincides with X degree isoseismal lines (Xu et al., 2020b). The 7,151 landslides triggered by the Haiyuan M8.5 earthquake in 1920 were distributed within the IX degree area (Xu et al., 2020c). In the Loess Plateau region of China, a large number of valleys, empty areas, and an arid climate have created favorable conditions for the formation and preservation of landslides due to earthquakes. Large-scale dense landslides triggered by historical strong earthquakes can be preserved for decades, hundreds, or even thousands of years. There is a significant difference in the scale between loess landslides due to rainfall and seismic landslides (Xu et al., 2020a). Based on the principle of "connecting the present to the past," the spatial distribution of preserved large-scale landslides can be used to determine the source parameters of historical strong earthquakes. Similar to analyzing present-day earthquake cases, we can use remote sensing interpretation technologies to perform detailed interpretations and investigations of landslides triggered by historical strong earthquakes, which yield determinations (or modifications) of the magnitude and epicenter parameters of historical earthquakes.

The 780 BC Qishan earthquake, which occurred along the southwestern margin of the Ordos Block in China, was the earliest destructive earthquake recorded in Chinese history. The "Book of Songs" and "Historical Records" clearly record that the earthquake occurred in the second year of King Zhou You. The ground damage included "three rivers exhausted, Qishan collapse, hundred rivers boiled, and hills collapsed". "The high banks turned into valleys," and "The deep valley became a mausoleum," among other accounts. These records indicate that the earthquake triggered a large number of coseismic landslides. According to these records, this earthquake was a strong event, such that it has attracted the attention of numerous researchers. However, there has been substantial debate over the magnitude of the Qishan earthquake, the macro-epicenter, the range of the extreme earthquake zone, and the seismogenic structure. Various earthquake catalogs have determined the location of the macro-epicenter of this earthquake in Qishan County, Shaanxi Province based on the "Qishan collapse." Scholars suggest that "Sanchuan" in "Sanchuan Exhaust" refers to the present day Jinghe, Weihe, and Luohe rivers. The magnitude is uncertain; various earthquake catalogs generally estimate the magnitude at 6 to ≥ 7. The epicenter intensity is also uncertain; the lack of a consensus yields uncertainty in the assessment of regional seismic activity and seismic risk analysis (Gu, 1983 and **Table 1**).

In addition to studying historical earthquakes on the edge of the Ordos block through limited historical records, a large number of landslides triggered by earthquakes also carry seismic parameter information (e.g., the AD 1303 Hongdong earthquake, AD 1556 Huaxian earthquake, AD 1654 Lixian earthquake, AD 1718 Tongwei Earthquake, and 1920 Haiyuan Earthquake) (Gu, 1983; Department of Earthquake Disaster Prevention, National Seismological Administration, 1995). Except for smaller landslides that have transformed and

TABLE 1 | Records of the 780 BC Qishan earthquake from different documents.

Literature	Estimated epicenter location	Estimated magnitude	Epicenter intensity	Remarks and references
"China Earthquake Catalog" 1960	Guanzhong (epicenter is ominous, likely not far from Qishan)	6–6.75		Sanchuan (Jinghe, Weihe, and Luohe rivers) (Li, 1960)
"China Earthquake Catalog" 1983	Qi'shan (34.5°N, 107.8°E)	6–7		Sanchuan (Jinghe, Weihe, Luohe and rivers). Unknown epicenter (Gu, 1983)
"A brief List of earthquakes in China" 1988	Qi'shan (34.5°N, 107.8°E)	6–7		
Catalog of Strong Earthquakes in Chinese History 1995	Qi'shan (34.5°N, 107.8°E)	≥ 7	≥ IX	Sanchuan (Jinghe, Weihe, and Luohe rivers) (Department of Earthquake Disaster Prevention, National Earthquake Administration, 1995)
"Catalog of Strong Earthquakes in four Provinces (Regions) of Shaanxi, Gansu, Ningxia, and Qinghai"	Qi'shan (34.5°N, 107.8°E)	6–7		Sanchuan (Jinghe river, Weihe river, Luohe river) (Lanzhou Institute of Earthquake Research, State Seismological Administration, 1985)
"Qishan county chronicles"	Qi'shan (34.5°N, 107.8°E)	6–7	VIII	Sanchuan (Jinghe, Weihe, and Luohe rivers)
National Earthquake Science Data Center, China Historical Earthquake Catalog	(34.5°N, 107.8°E)	6.5		

disappeared, larger landslides remain clearly visible on remote sensing images. A large number of dense historical loess landslides are currently preserved along the southwestern margin of the Ordos Block.

This study attempts to implement the interpretation methods detailed in the current strong earthquake landslide survey, combined with a historical literature review and field surveys, and uses current remote sensing images to interpret, in detail, historical landslides along the southwestern margin of the Ordos block. Based on dating results of existing bedrock collapses and loess landslides, historical landslides in the dense area along the southwestern margin of the Ordos block can be linked to the 780 BC Qishan earthquake. In addition, we discuss the possible magnitude, epicenter location, seismogenic structure, and earthquake damage scale associated with the 780 BC Qishan earthquake based on the distribution of landslides.

MATERIALS AND METHODS

Geological Background

The southwestern margin of the Ordos Block has a special structural location, i.e., it is at the forefront of the northeastward expansion of the Tibetan Plateau (**Figure 1**) (Yuan R et al., 2013; Zheng et al., 2013; Zheng et al., 2017; Li, 2018). This area experiences strong tectonic activity and frequent occurrences of both strong historical and current earthquakes. The southwestern margin of the Ordos Block is one of the areas where casualties are extremely tragic (Peng, 1992). The AD1654 Lixian *M*8 earthquake caused 30,000 deaths (Yang et al., 2015). The AD1718 Tongwei M7.5 earthquake caused more than 70,000 deaths, and there is a clear record that a considerable number of deaths are related to the earthquake landslide (Sun et al., 2017). The AD1920 Haiyuan *M*8.5 earthquake caused 270,000 deaths (Cheng et al., 2017), of which more than 100,000 deaths may be directly related to the earthquake landslide (Li et al., 2015). At the same time, this area is a danger zone for strong earthquakes in the future. GPS deformation observation results show that since 1920, the remaining seismic moments on the southwestern margin of the Ordos Block have been accumulating and have been in a state of loss, which has the potential to generate Mw ≥ 7 earthquakes (Li, 2019). The Liupanshan Fault zone and Longxian–Baoji Fault zone are the main fault zones along the southwestern margin of the Ordos Block. Ye et al. (2018) used GPS data inversion to examine the northern section of the Longxian–Baoji Fault zone, finding that this area is in a highly closed state with a greater seismic risk. Previous studies suggest that the middle–south section of the Liupanshan Fault zone and Longxian–Baoji Fault zone are two dangerous areas where strong/major earthquakes may occur in the future. Magnitude estimates of possible earthquakes along the Liupanshan and Longxian–Baoji Fault zones are Mw 7.3 and 7.2, respectively (Du et al., 2018). The Longxian–Qishan–Mazhao Fault is the most active fault in the Longxian–Baoji Fault zone, with a total length of approximately 180 km. This fault is a late Quaternary active fault with an overall NW trend. The fault is mainly left-lateral sliding, accompanied by a certain normal fault (Li, 2018).

Landforms along the southwestern margin of the Ordos Block can be mainly divided into three components: mountains formed by bedrock, the Loess Plateau, and the Weihe Basin. The mountain ranges composed of bedrock include uplift areas, such as Liupan Mountain, Longshan Mountain, Qinling Mountain, Qianyangling Mountain, and Beishan Mountain. They are mainly Precambrian metamorphic basement, granite

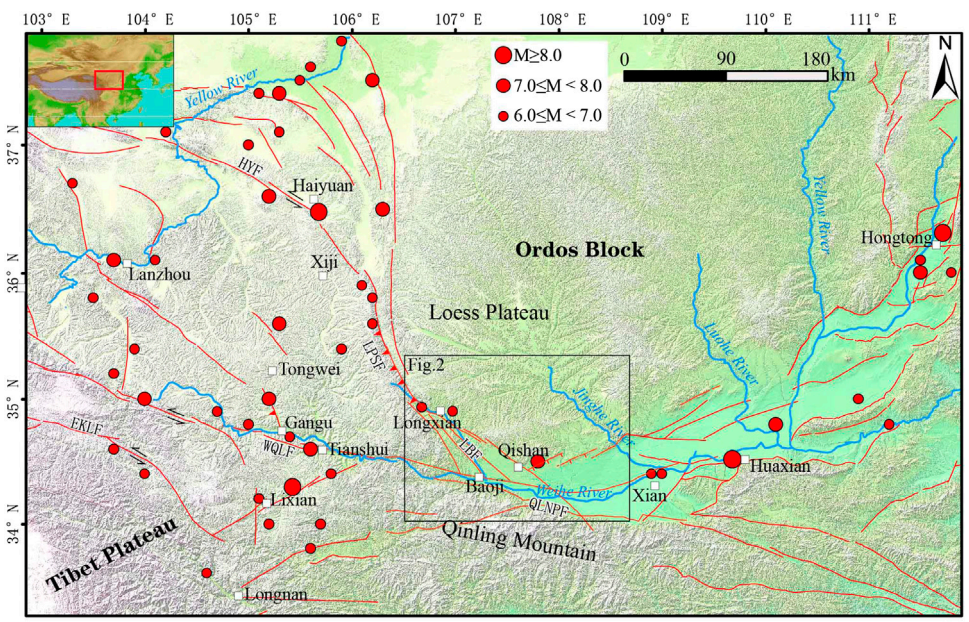

FIGURE 1 | Regional background map. LBF: Longxian Baoji Fault Zone; LPSF: Liupanshan Fault; HYF: Haiyuan Fault; WQLF: West Qinling Fault; EKLF: East Kunlun Fault; QLNPF: West Qinling North Margin Fault; The black box represents the range of **Figure 2**.

bodies, Paleozoic strata, and some Mesozoic strata. The Loess Plateau is covered by Quaternary aeolian loess-paleosol, with thicknesses reaching from 120 to approximately 180 m. The main components of loess are silt or clay, characterized by loose, easily erodible soil. The Loess Plateau is one of the regions with the most serious soil erosion in the world (Li et al., 2019). The eroded landform types include plateaus, beams, and ridges. The terrain is undulating, ravines are vertical and horizontal, and mountains are high and steep. These characteristics create excellent terrain conditions for the occurrence of landslides. The Weihe River Basin includes various levels of loess tableland and Weihe river terraces. The loess plateaus are flat and do not have topographical conditions appropriate for dense landslides.

From the late Holocene to the present, the Baoji area on the southwestern margin of Ordos has been affected by global climate change, the climate has become colder, the intensity of the summer monsoon has weakened, and the winter monsoon has increased. The climate has entered a phase of relatively cold, arid, and scarce precipitation (Deng, 2011). The dry climate along the southwestern margin of the Ordos Block is conducive to the preservation of loess landslides.

Interpretation Method

Satellite images taken before and after earthquakes can be used for detailed interpretation of landslides after modern major earthquakes. The image data used to interpret historical earthquake landslides must conform to the two following requirements: 1) the resolution of the image should be sufficiently high to facilitate the identification of the range of each part of the landslide body through user experience and 2) the area should be covered by the maximum number of temporal images to facilitate comparative interpretations. The interpretation of historical landslides is based on the following. 1) Current earthquake case studies show that only large earthquakes can trigger dense landslides; larger landslides can be preserved for extended periods (Xu et al., 2020a). The scale of landslides caused by moderate earthquakes is limited which has a negligible impact on the interpretation of landslides caused by large earthquakes (Du et al., 2020a). 2) Seismic landslides and rainfall-triggered landslides have distinct characteristics with respect to their duration, area scale, and distribution (Xu et al., 2020a). 3) Large-scale artificially-induced landslides appear as single points or distributed across residential areas; these are also significantly different from dense large-scale landslides. 4) We cannot overlook that earthquake landslides occurred before rainfall or human activity-induced landslides; however, the overall shapes between these landslide types remain clearly distinguishable. We used high-resolution satellite images from Google Earth to systematically interpret historical landslides in the study area and surroundings. Google Earth can provide multi-temporal images with different resolutions of up to 0.15 m. We used Google Earth images of the study area collected from 2005 to 2018, with resolutions of 1–5 m; most areas had an image coverage of more than three times. Google Earth supports a 3-D display at any angle, such that the shape and outline of the landslide can be clearly distinguished. To understand the completeness of the translation, we interpreted it on a river-by-basin basis. In addition, domestic high-resolution satellite images collected by the GF-1, GF-2, and American Keyhole satellites from the 1960s to the 1970s were used as supplementary data sources. If some parts of Google Image are covered by clouds, etc., we used domestic high-resolution satellite image as supplementary data. The Keyhole historical satellite images as a supplementary data source can eliminate the impact of landslides caused by human activity in recent decades. Later field excursions were also used to verify the accuracy of the interpretations. Using Google Earth images, we manually extracted and saved the boundaries of the target landslides as vector files in a kml format. Attribute information for the landslide body was assigned using ArcGIS software. The attribute information included the length and width of the landslide, the elevation of the scarp top and foot edge, and the top and bottom elevations of each located slope.

RESULTS

Interpretation Results

The landslides in the study area had the following image characteristics. 1) There are abnormal arc shapes developed on the rear margin of the landslide body, including "round chair-shaped" and "dustpan-shaped" landslide back wall steep ridges, curved terrain variation lines, and abnormal color lines, among other feature. 2) Landslides protruding toward the bottom of the valley often have slight topography. Landslides often form dammed lakes in the valleys, which occasionally discharge water. The original "V"-shaped loess valley bottom becomes flat terrain, which has been mostly transformed into cultivated land. 3) Most landslides are distributed in the partial deficit areas of steep slopes, such as valleys and rivers. Landslides cause river water to shift to the side of the river where the landslide has not occurred. 4) The valley slopes on both sides of the steep loess valley have abnormally flat cultivated land.

In this study, the historical landslides in the 28,000 km^2 area of the southwestern edge of Ordos was interpreted in detail. **Figure 2** shows the spatial distribution of the interpreted historical landslides. The landslides are mainly distributed along faults to the north of the Longxian–Qishan–Mazhao Fault, east of Longxian, south of Lingtai, and the uplift area of the fault block south of Qianyang. There are 6,876 landslides in this dense area, with a total area of 643 km^2. There are relatively few dense landslides on the Loess Plateau, Weihe river terraces, and floodplains on the southwest side of the Longxian–Qishan–Mazhao Fault due to topographical conditions. At the same time, dense landslides were not interpreted in the bedrock area of the Qishan mountains and north of Fengxiang.

The area density analysis of the interpreted landslides in the study area (**Figure 3**) shows that, although there are landslides in the study area, the high-density areas occur on the northeastern side of the Longxian–Qishan–Mazhao Fault. The area density can reach as high as 28–35% while the area density value at the center of the high-density area is 4- to 5-fold greater than the background density of the Loess Plateau, highlighting this as an abnormal area.

The 6,876 landslides in the dense area were projected onto the projection line along the horizontal and vertical strike of the

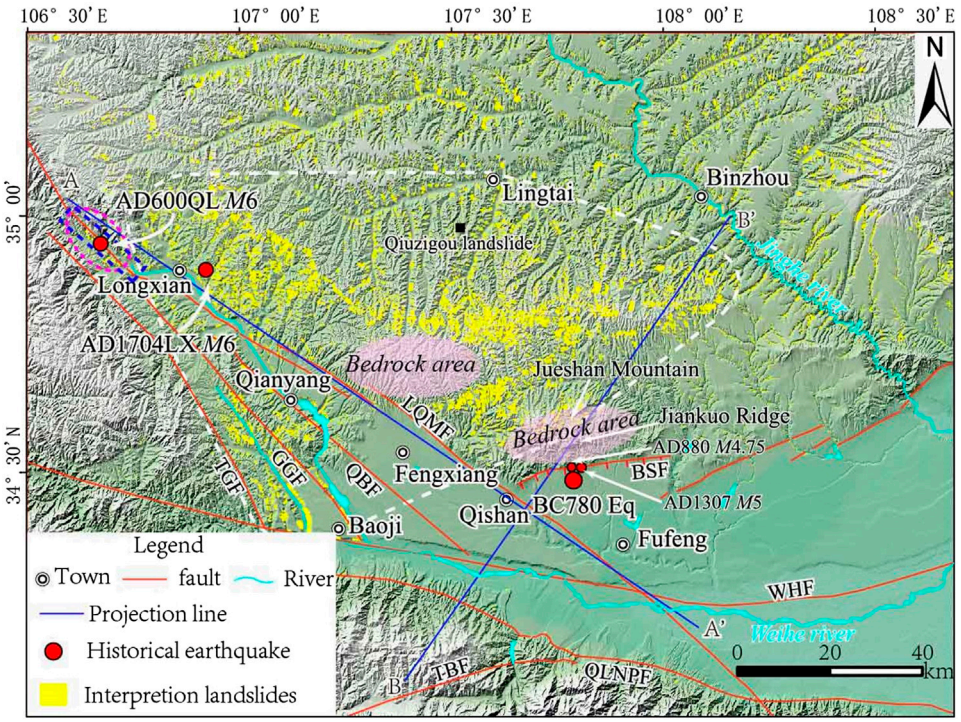

FIGURE 2 | Interpreted historical landslide distribution map at the Southwest of Ordos. LQMF: Longxian–Qishan–Mazhao Fault; QBF: Qianyang–Biaojiao Fault; GGF: Guguan–Guozhen Fault; TGF: Taoyuan-Guichuansi Fault; QLNPF: Qinling North Margin Fault; TBF: Taibai Mountain Fault; WHF: Weihe Fault; and BSF: Beishan Piedmont Fault. The purple dashed oval area is the extreme earthquake zone of the AD 600 Qinlong earthquake (Wang, 2018); the blue dashed rectangle represents the surface rupture of the AD 600 Qinlong earthquake along the Longxian–Qishan–Mazhao fault of the Dazhuangke–Dengjiacao section (Li et al., 2019); the area denoted by the white dotted line is the dense landslide area; and projection lines A–A′ and B–B′ correspond to **Figure 4**.

Longxian–Qishan–Mazhao Fault; we then counted the frequency and cumulative area of the landslides (at 10 km intervals) (**Figure 4**).

Along the strike of the Longxian–Qishan–Mazhao Fault, landslides are mainly concentrated within a range of 90 km between Longxian and Qishan (reaching 6,003 events, accounting for 87.3% of the total number of landslides). The cumulative landslide area is 557.4 km^2, accounting for 86.7% of the total landslide area. The peak appears at approximately 10 km northwest of Qishan County. By projecting the landslide body onto the projection line perpendicular to the strike of the Longxian–Qishan–Mazhao Fault, we observe that the main body of the landslide is distributed on the northeast side of the Longxian–Qishan–Mazhao Fault, where there is a sharp reduction in the number and area of landslides southwest of the fault. This is because the southwest side of the fault is the loess tableland and Weihe River terraces and floodplains, which do not have topographical conditions suitable for large-scale landslides. The landslide-intensive area is distributed unilaterally along the Longxian–Qishan–Mazhao Fault.

Landslide Database and Parameter Statistics

Based on our interpretations, parameter assignments were made for the landslides in dense areas on a case by case basis to establish a coseismic landslide database. The manually assigned attributes of the landslide database included the length, width, elevation of the scarp top and foot edge, and the top and bottom elevations of each located slope. Accorded to these assigned attributes, we calculated several landslide attributes, including the landslide height, H (elevation of the scarp top-elevation of the foot edge), slope difference (the top and bottom elevation difference of each located slope), aspect ratio, and landslide height/slope difference ratio, i.e., H/(R − V).

A statistical analysis of the landslide parameters was conducted based on the coseismic landslide database. The length advantage interval of the historical landslides in the dense area along the southwestern margin of the Ordos Block is 100–500 m; this interval accounts for 82% of the total number of landslides. The width advantage interval is 100–400 m; this interval accounts for 72.6% of the total number of landslides (**Figures 5A**,**B**). The aspect ratio of the landslide represents the plane spread of the landslide, which ranged from 0.1 to 5.6 for the historical landslides in the dense areas, mainly concentrated between 0.5 and 2.5. This interval accounts for 91% of the total landslides. An aspect ratio of ≤ 0.5 accounted for 5.6% of the total landslides while an aspect ratio of >2.5 accounted for 3.4% of the total landslides, with an average of 1.25 (**Figure 5C**).

The term H/(R − V) refers to the ratio of the height, H, of a landslide to the slope difference (R–V: Ridge–Valley), which represents the ratio of the longitudinal length of the landslide to the slope length where the landslide is located, ranging from 0 to 1. The greater the value of H/(R − V), the greater the proportion of

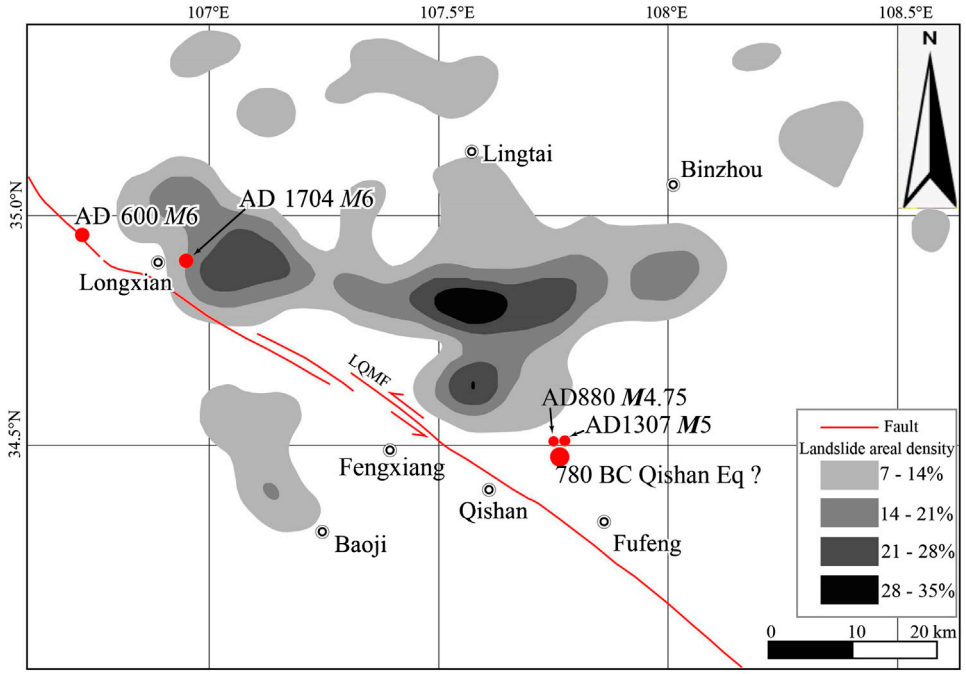

FIGURE 3 | Interpreted historical landslide areal density map. LQMF:Longxian–Qishan–Mazhao Fault; AD 600 M6:AD 600 Qinlong M6 earthquake; AD 1704 M6: AD 1704 Longxian M6 earthquake;

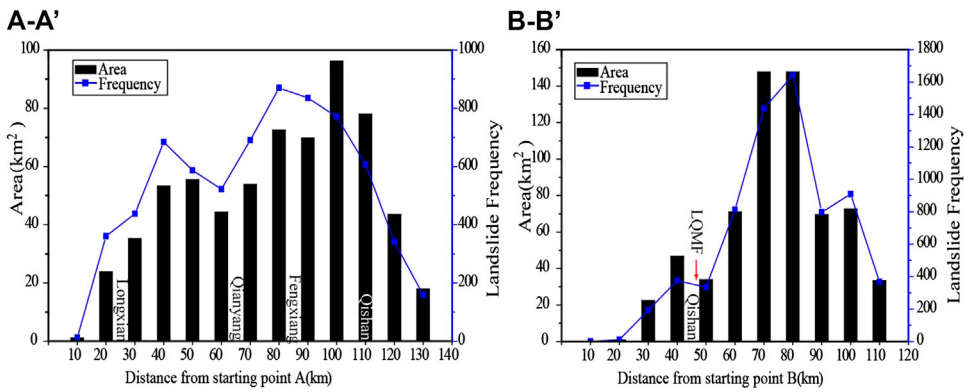

FIGURE 4 | Frequency and cumulative area along strike and vertical strike of the Long xian–Qishan–Mazhao Fault (10 km) (Projection lines A–A′ and B–B′ are shown in **Figure 2**).

landslides in the slope in the longitudinal direction. Among the landslides in the dense areas, 85.4% of landslides have H/(R − V) ratios >0.6 while 57.7% are greater than 0.8 (**Figure 5E**). This shows that the scarp tops of these landslides basically reach the Loess Plateau, with notable landform deficits While the foot edge accumulation basically reaches the bottom of the valley, which can lead to the damming of loess valleys at different scales, forming abrupt landform sedimentary features; these features are consistent with the observation results collected during the field survey (**Figures 6A–D–D**).

In terms of the area, the number of small-area landslides is relatively small; landslides with an area greater than 10,000 m^2 account for 93.2% of the total number of landslides. The area advantage of historical landslides interpreted in the study area is 10,000–200,000 m^2; the number of landslides in this section accounts for 82.3% of the total number of landslides in the dense area of this study (**Figure 5D**).

DISCUSSION

Dense Historical Landslides and the 780 BC Earthquake

In addition to the 780 BC Qishan earthquake, the AD 1704 Longxian earthquake and AD 600 Qinlong earthquake occurred in the study area (**Figure 2**).

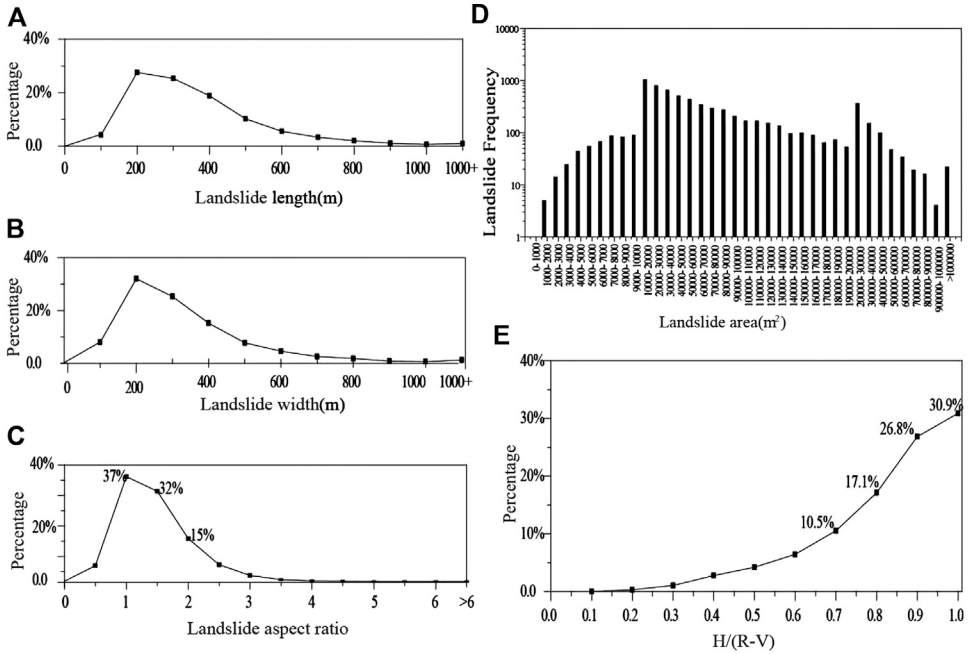

FIGURE 5 | Landslide parameter statistics. **(A)**, statistics on the relationship between landslide length and frequency; **(B)**, statistics on the relationship between landslide width and frequency; **(C)**, statistics on the relationship between landslide aspect ratio and frequency; **(D)**, statistics on the relationship between landslide area and Frequency; **(E)**, statistics on the relationship between landslide H/(R – V) and frequency.

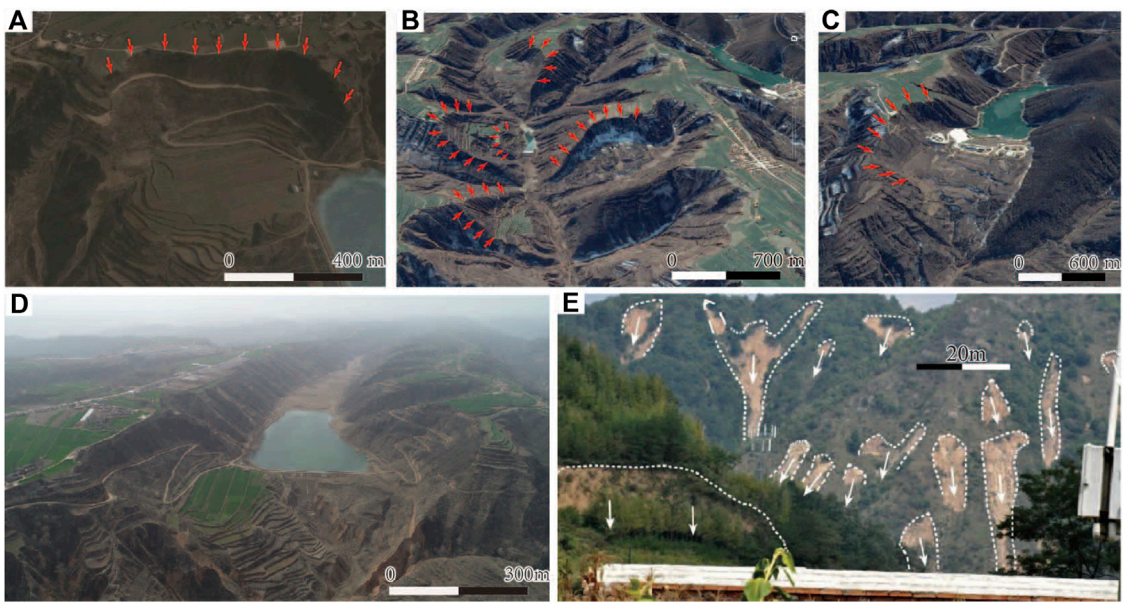

FIGURE 6 | Google images of typical historical landslides and barrier lakes **(A–C)**, UAV. photos of historical landslides(d), and photos of rainfall landslides **(E)**.

Wang (2018) suggested that the seismogenic structure of the AD 600 Qinlong earthquake was due to the Guguan-Caojiawan section of the Liupan Mountain East foot Fault based on an ancient seismic exploration trough, collapsed body, and formation time. Li et al. (2019) proposed that the epicenter of the AD 600 Qinlong earthquake was located 15 km (34.9°N, 106.7°E) northwest of Long County. The epicenters (highly seismic regions) reported in the above two most recent studies are close, providing sufficient evidence. Therefore, we consider that the epicenter of the AD 600 Qinlong M6 earthquake was

15 km northwest of Longxian County (**Figure 2**). For the AD 1704 Longxian earthquake, The "China Earthquake Catalog" (Gu, 1983), published in 1983, set the earthquake at a magnitude of 6, with an epicenter intensity of VII–VIII. As there are relatively few research results on this earthquake, we consider that the epicenter of the AD 1704 Longxian M6 earthquake was in the vicinity of Longxian based on the historical earthquake catalog (Gu, 1983).

In addition to the 780 BC earthquake, there were two earthquakes at a magnitude of approximately 5 that occurred in AD 880 and AD 1037 along the southwestern margin of the Ordos Block. According to the historical descriptions of "Three rivers exhausted, Qi mountain collapse," "Hundred rivers boiled, mountain mounds collapsed. High banks turned into valleys, and deep valleys turned into tombs" recorded in "Book of Songs" and "Historical Records", the damage intensity and scope of the "780 BC Qishan Earthquake" were greater than those of the other two earthquakes. The relevant historical earthquake catalog also sets the magnitudes of these two historical earthquakes in AD 880 and AD 1037 as 4.75 and 5, respectively. Therefore, considering the limited energy of moderate and strong earthquakes, we suggest that the two most recent historical earthquakes, i.e., the "Qishan collapse" and "Qishan collapse again," were only records of earthquake occurrences, not triggers of a large number of landslides. Moreover, the most recent historical earthquakes were more than 1,500 years after the 780 BC earthquake. If the earthquake that triggered the "Qishan collapse" really occurred, records of earthquake damage should theoretically be more abundant than those for the Qishan earthquake in 780 BC; however, there are no other relevant records on these two earthquakes.

According to the interpretation and cataloging results of landslides triggered by earthquakes at a magnitude of approximately 6 (**Table 2**), the scale of landslides triggered by these earthquakes is limited and the range of dense landslides is small. Therefore, although a small part of the landslides at the northwest end of the landslide distribution range in the study area may have been triggered by the AD 600 Qinlong and AD 1704 Longxian earthquakes, the proportion is small and the impact range is limited. The main landslides in the dense area cannot have been triggered by these two earthquakes.

Analyses of the landslides triggered by the Wenchuan earthquake indicate that the far-field effect of strong earthquakes will not trigger large dense landslides outside the extreme earthquake zone (Xu et al., 2014; Du et al. 2020a). Several large earthquakes outside the landslide distribution range are far from the landslide dense area (**Table 3**), such that the possibility of large dense landslides triggered by strong earthquakes outside the range is negligible.

The age of a single landslide is the most powerful evidence to establish a connection between landslides and historical earthquake. Zhou et al. (unpublished, 1993) used lichen geochronology technologies to date 382 bedrock collapses in the Jiankou ridge and Jueshan Mountain region (**Figure 2**). The results showed that the huge collapses in this region were caused by the 780 BC Qishan earthquake. The age of the sediment at the bottom of the landslide dammed lake can represent the age of the landslide. Du et al. (2020b) selected a typical Qiuzigou landslide dam (**Figure 2**) in the study area and obtained ^{14}C dating samples in the bottom sediment of the dammed lake through drilling. These samples are measured by American Beta Laboratories using an accelerator mass spectrometer. The dating results are close to the Qishan earthquake time. Combined with the above age results and comprehensive analysis, we believe that the main body of the dense landslides was most likely caused by the 780 BC Qishan earthquake.

"Incomplete" Historical Landslide Database

Comparing the area–frequency relationship between historical landslides in the dense area (inside the white dotted line in **Figure 3**) along the southwestern margin of the Ordos Block and the Wenchuan earthquake landslide (Du et al., 2020a) (**Figure 7**), there are large differences in the number of landslides in different area intervals. The number of historical landslides in the dense area along the southwestern margin of the Ordos Block is small, ranging from 1 to 10,000 m^2 with only 469 landslides (approximately 6.8% of the total), while the number of landslides due to the Wenchuan earthquake is 32,007, accounting for 61% of the total. This significant difference in the proportion of landslides of <104 m^2 reflects that with the passage of time, small-to-medium-scale historical landslides have basically "disappeared" due to surface processes and man-made transformations, such that they can no longer be identified on current remote sensing images. In particular, the smaller landslides are increasingly rare.

In the 2008 Wenchuan earthquake, small landslides, which accounted for a large proportion of the total, contributed little to the total area of landslides induced by the earthquake (**Figure 8**) (Du et al. 2020a). Large-scale landslides that can be identified today may represent the main body of a historical earthquake landslide; they can also reflect the overall scale of a historical earthquake landslide. Therefore, we discuss medium- and large-scale historical landslides in the dense area along the southwestern margin of the Ordos Block.

In August 2010, partial heavy rain in southeastern Tianshui that triggered a large rainfall landslide. These landslides are generally small in scale, mostly slippery on their slopes, and have a short duration. Rainfall landslides that occurred in 2010 could not be identified in remote sensing images taken after 2016. Some rainfall landslides develop on the back or sidewalls of large earthquake landslides, or on the ridges of loess terraces that have been transformed by humans (Xu et al., 2020a). Xu et al. (2020b) used historical document analysis, remote sensing interpretation, field verification, and other methods to interpret 5,019 landslides triggered by the AD 1718 Tongwei earthquake on both sides of the Tongwei Fault, with a total area of 635 km^2. As this earthquake landslide has clear historical records, it can be used as a typical example of a loess earthquake landslide.

Comparing the area–quantity relationship between historical landslides in dense areas (inside the white dotted line in **Figure 3**), the 2010 Tianshui rainfall landslides, and the AD 1718 Tongwei earthquake landslide (**Figure 9**), rainfall landslides mainly have areas of <10,000 m^2, accounting for 99% of the total landslides. However, there are few small-area landslides in the

TABLE 2 | Interpretation and cataloging results of landslides triggered by earthquakes of approximately M6.

Earthquake cases	Intensity at macro-epicenter	Distribution scale (km)	Size of landslides	References
2013 Minxian M6.6	VIII	Narrow belt, < 15	Small (total area of 1.71 km^2)	Xu et al. (2013)
1970 Xiji M5.5	VII–VIII	4–5	Small	Wang (2003)
1936 Kangle M6 ¾	VIII	8	Rock falls	Zhang et al. (2015)
1936 tianshui town M6.0	VIII	–	Not clear record	Wang et al. (2018)
1837 Minxian M6.0	VIII	–	Not clear record	Zheng et al. (2007)
AD 1125 Lanzhou M7.0	IX	~7	Landslides along the fault	Song et al. (2007)

TABLE 3 | Basic parameters of three historical strong earthquakes around Qishan Longxian and the impact of the earthquake on Qishan Longxian.

Historical earthquake	Distance to landslide dense area (km)	Triggered landslides	Impact of the earthquake on Qishan Longxian	References
1,556 Huaxian *M*8.0	200	The east and west ends of the Huashan Piedmont fault zone	(Qishan) The city, government offices, temples, and houses were destroyed, and the people were crushed to death; (Fengxiang) many people and animals were crushed to death; (Linyou) Destruction of confucian temple	Xu et al. (2018)
1,654 Lixian *M*8.0	190	Between Tianshui Town and Li County	(Baoji) "House destruction, crushing people"; (Fufeng) "Gyeongbok Palace, Yuanyu collapsed, crushing people and animals." (Lin You) "Kilins collapsed, crushing people and animals."; (Qishan, Feng Xiang) "The walls and houses burst up, people and animals can't stand in shock"	Yuan et al. (2017)
1920 Haiyuan *M*8.5	250	Xiji, Haiyuan, Longde area	The Qishan wall collapsed, the ground was cracked and deep gully, people were killed and injured everywhere	Li et al. (2015)

dense areas and within the landslides triggered by the AD 1718 Tongwei earthquake. Landslides with areas >10,000 m^2 accounted for 93.2% and 88.7% of the total in the dense areas and due to AD 1718 Tongwei earthquake, respectively. Therefore, the remaining historical landslides in this study and rainfall landslides can be distinguished by size.

Comparing the length, width, and aspect ratio of historical landslides in the dense area (within the white dotted line in **Figure 3**) with the 2010 Tianshui rainfall landslide and the AD 1718 Tongwei earthquake landslide (**Figure 10**), we observe that 88.4 and 98.9% of the rainfall landslides have a length of ≤100 m and a width of ≤100 m, respectively. The lengths and widths of the historical landslides in dense areas are similar to those of the AD 1718 Tongwei earthquake. Landslides with a length ≤100 m accounted for only approximately 4.2 and 7.2% of the total while landslides with a width ≤100 m accounted for only approximately 7.9 and 14.4% of the total, respectively.

The aspect ratio of historical landslides in dense areas is similar to that of the AD 1718 Tongwei earthquake landslides, mainly between 0.5 and 2.5; landslides in this interval accounts for 89.1% of the total landslides. There is a significant difference between the 2010 Tianshui rainfall landslide and the two earthquakes mentioned above. The landslide aspect ratio for the 2010 Tianshui rainfall landslide ranged from 0.03 to 57.18, with an average value of 3.06. The aspect ratios of rainfall landslides mainly range from 0.5 to 4. The landslides in this interval account for 71% of the total; aspect ratios ≤0.5 account for 5.5% of the total while aspect ratios >4 account for 23.5% of the total, indicating that most rainfall landslides are long and narrow (**Figure 10C**).

Compared with rainfall landslides, there are notable differences with historical landslides in dense areas in terms of their areas, lengths, and widths. The dense historical landslide is highly similar to the AD 1718 Tongwei earthquake landslide in terms of their areas, lengths, and widths. Therefore, there is a clear macroscopic difference between historical earthquake landslides and rainfall landslides. The main part of the landslides in the dense areas was not likely triggered by rainfall events but was more likely triggered by earthquake events. Strong earthquakes can cause such a large-scale landslide. Several earthquakes of magnitudes ≤5 have occurred in the landslide-intensive area and did not trigger large-scale landslides.

Rainfall landslides that occur on the Loess Plateau are generally small in scale and short-lived. Usually, the landslide will be transformed with the restoration of surface vegetation and human activities a few years after its occurrence, such that they can no longer be identified in high-resolution satellite images. Medium- and large-scale landslides triggered by earthquakes will cause significant changes in local landforms, which generally endure for an extended period. Although various natural and man-made modifications may have contributed to these landslides, their basic shapes can still be identified (Xu et al., 2020b).

We note that the previous discussion only points out the differences between historical earthquake landslides and rainfall landslides from a macro perspective. Individual large-scale rainfall landslides may be characterized by continuous activity;

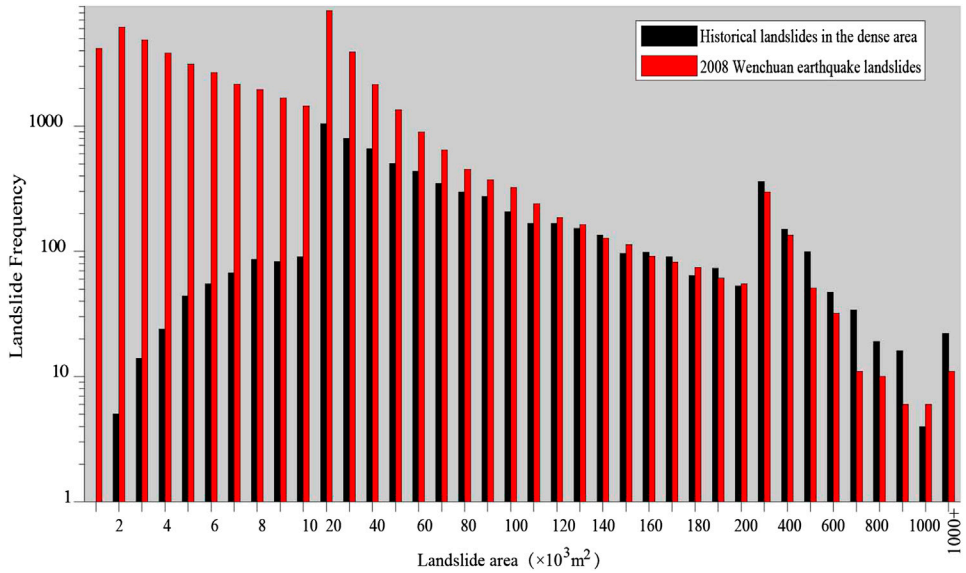

FIGURE 7 | Comparison of the area-frequency relationship between the Qishan earthquake landslide and Wenchuan earthquake landslide.

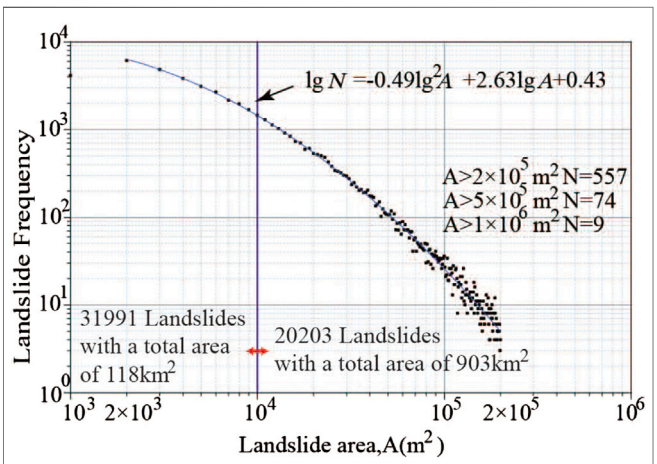

FIGURE 8 | Relationship between the cumulative number and area of landslides in the Wenchuan earthquake (Du et al., 2020a).

large-scale earthquake landslides may also be characterized by continuous activity due to rainfall after the earthquake.

Regional Control Characteristics of Strong Historical Earthquake Landslides

The landslides in the dense area are mainly distributed along the north side of the Longxian–Qishan–Mazhao Fault with an asymmetric distribution. According to the analysis, the Loess Plateau and river terraces lie toward the southwest side of the fault while the Loess Plateau and mountain hills lie toward the northeast side. Limited by topographical conditions, dense landslides do not occur on the southern and western sides of the fault; therefore, "sand liquefaction" and "seismic soil" will more likely form in soft areas, such as river terraces and valleys, due to violent earthquake vibrations (**Figure 11**). According to the characteristics, landslides triggered by strike-slip fault activities are mainly distributed on both sides of the fault (Chen et al., 2014). If the geological engineering conditions on the south side of the Longxian–Qishan–Mazhao Fault are the same as those on the north side, there may also be dense historical landslides.

780 BC Qishan Earthquake Parameters

The 780 BC Qishan earthquake is an earthquake that is historically difficult to interpret, with a long elapsed time and unknown historical records. Determining the intensity/isoseismic distribution is difficult. However, for a major earthquake that triggers a secondary disaster, the range of its extreme earthquake zone/severely damage zone can be obtained through the spatial distribution and characteristics of secondary disasters revealed by high-resolution remote sensing images. The center of the macroscopic damage zone is the macroscopic epicenter. Therefore, the epicenter of the 780 BC Qishan earthquake may be located northwest of Qishan, closer to Fengxiang.

The Longxian–Qishan–Mazhao Fault has been the most active fault in the Longxian–Baoji Fault zone since the late Quaternary. The National Earthquake Administration (1988) divided the fault into three sections: Xinjichuan–Longxian section, Longxian–Qishan section, and Qishan–Mazhao section. Historical landslides in dense areas are mainly concentrated in the range of 90 km between Longxian and Qishan, corresponding to the Longxian–Qishan section of the Longxian–Qishan–Mazhao Fault.

The extension of the severe damage zone of a major earthquake along the seismogenic fault can represent an extension of the fracture. The surface rupture zone produced by the Wenchuan earthquake spread within the IX intensity zone.

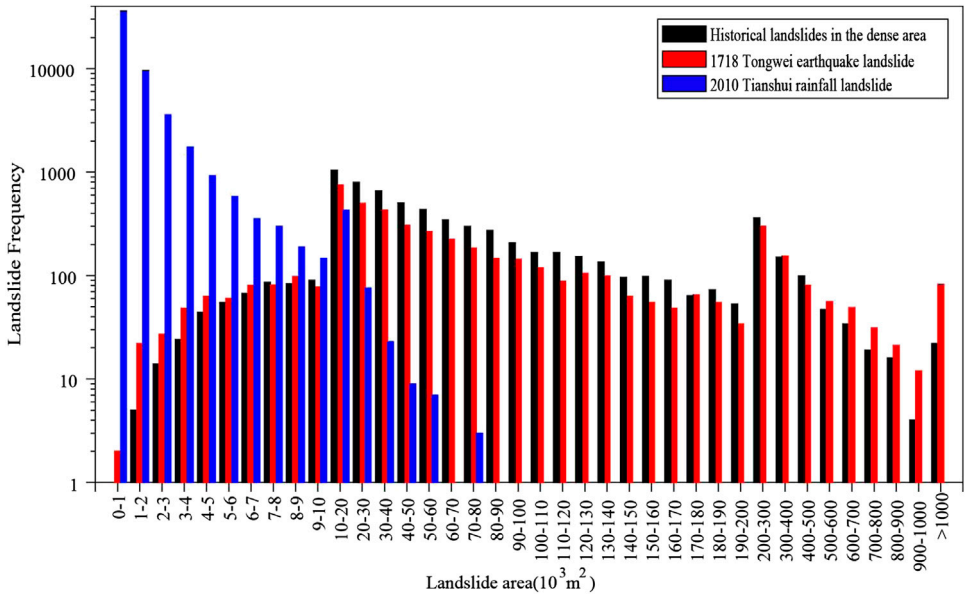

FIGURE 9 | Comparison of the dominant area of the rainfall landslide and the 1718 Tongwei earthquake landslide (Xu et al., 2020a; Xu et al., 2020b) and the historical landslide area in Long County, Qishan

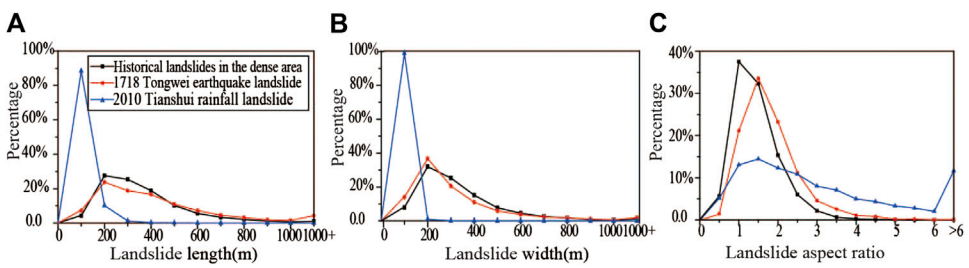

FIGURE 10 | Comparison of the lengths, widths, heights, and aspect ratio of landslides: **(A)** comparison chart of landslide lengths; **(B)** comparison chart of landslide widths; and **(C)** comparison chart of landslide aspect ratios.

The area of landslides within the IX zone accounted for 81.1% of the total area, and the number of landslides in the IX zone accounted for 76.9% of the total landslides. We suggest that the landslide-intensive area within a range of 90 km between Long and Qishan Counties can represent the rupture area of the 780 BC Qishan earthquake, as well as the severely damaged area. Therefore, the minimum possible rupture length for the rupture zone of the 780 BC Qishan earthquake was 90 km.

We assumed that the Longxian–Qishan section of the Longxian–Qishan–Mazhao Fault is completely broken. According to the global empirical formula, i.e., Mw = 5.16 + 1.12lgL (Wells and Coppersmith, 1994), for the rupture length and magnitude of strike-slip faults, the moment magnitude is Mw 7.35 According to the empirical formula, i.e., M = 5.303 + 1.181lgL (Ran, 2011), for the strike-slip fault magnitude-fracture parameter in western China, the magnitudes is 7.61. According to the empirical formula, i.e., Ms = 5.704 + 0.9871lgL (Sun et al., 2016), the surface wave magnitude is Ms 7.63.

The earthquake disasters due to six strong earthquakes of magnitude 8 on the Loess Plateau are comparable to the 780 BC Qishan earthquake. For example, for the AD 1739 Ningxia Pingluo and Yinchuan *M*8 earthquake that occurred on the plains, there were no records of landslides, but the other five earthquakes produced documented landslides. The six *M*8 earthquakes have records of spring overflowing/river overflowing similar to the "boiled rivers" (**Table 4**). This shows that the intensity of the 780 BC Qishan earthquake may have been similar to the six *M*8 earthquakes.

For the magnitude of the 780 BC Qishan earthquake, except for the "Catalog of China's Historical Strong Earthquakes" published in 1995, which set the magnitude as ≥ 7, other historical earthquake catalogs all set the magnitude at 6–7. Based on the distribution and scale of landslide disasters, we posit that the magnitude of the 780

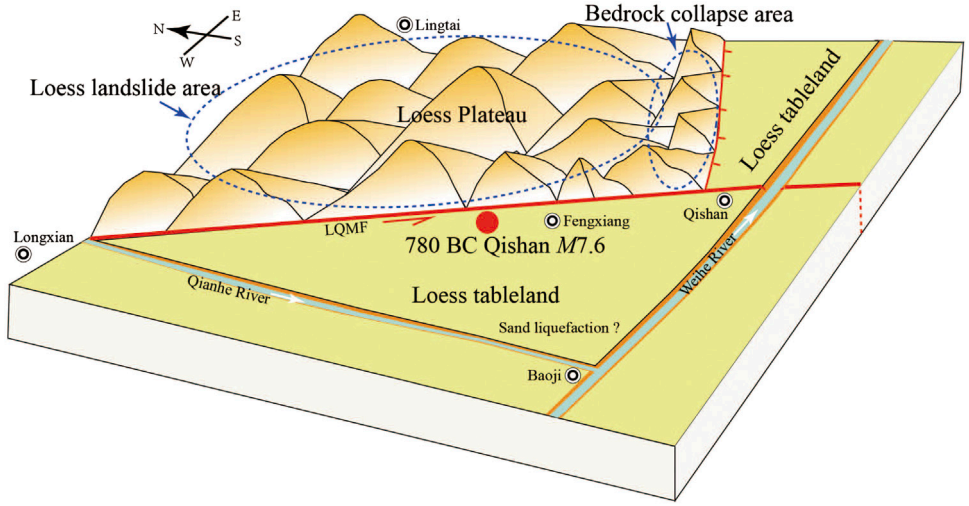

FIGURE 11 | Relationship between the distribution pattern of landslides in the dense area in this study and the 780 BC Qishan earthquake.

TABLE 4 | Historical records of earthquake damage due to 6 strong M8 earthquakes in or around China's Loess Plateau (Gu, 1983).

Historical earthquake	Phrases that appear numerous times in records of earthquake geological disasters
780 BC Qishan *M*7.6	Three rivers are exhausted, Qishan falls/Hundred rivers boil, and hills collapse. High banks become valleys, deep valleys become mausoleums
1,303 Hongtong *M*8.0	Ground fissure/ground gushing sand/water/city subsidence/landslide
1,556 Huaxian *M*8.0	Water surges and sand overflows/mountains move, ground rifts/mountains are exhausted/wells are exhausted, Luohe and Weihe rivers can be waded/landslides and rivers surge
1,654 Tianshui *M*8.0	Landslides and water stagnated, blocked as river ponds/ground fissures/gushing water
1739 Yinchuan *M*8.0	Ground fissure/city subsidence/gushing yellow sand and black water
1879 Wudu *M*8.0	Mountain fissure/water surge/landslide/landslide/river choked, then re-washed, the water was turbulent
1920 Haiyuan *M*8.5	The ground may become high tombs or sink into deep valleys, landslides and ground fissures, cliffs and landslides/blocked rivers/gushing water belts, black sand/mountains move away, peaks and valleys interchange/loess landslides/landslides

BC Qishan earthquake should be higher than the magnitude reported in the historical earthquake catalog, i.e., a magnitude of approximately 7.6 (Mw7.3). This is similar to the maximum moment magnitude Mw7.2 ± estimated by Du et al. (2018) for potential earthquakes in the Longxian–Baoji Fault zone.

CONCLUSION

Combining historical records and referring to current interpretation methods for strong earthquake landslides, we used high-resolution Google Earth images to extract historical landslides along the southwestern margin of the Ordos Block.

The results showed that there are 6,876 historical landslides in the landslide-intensive area along the southwestern margin of the Ordos Block, with a total area of 643 km^2. The landslide-intensive areas are mainly distributed unilaterally along the Longxian–Qishan–Mazhao Fault in the loess valley area on the northeast side of the fault. The southwest side of the fault is Loess Pateau and river terraces; owing to the topographical conditions, there is no dense landslide distribution in this area. Through a comprehensive analysis, combined with the dating results of existing landslides and bedrock collapses, the dense historical landslides on the southwestern margin of the Ordos Block were linked with the 780 BC Qishan earthquake. According to studies of landslides due to the Wenchuan earthquake, large-scale landslides in dense coseismic landslide areas can represent the main body of coseismic landslides. Finally, according to the spatial distribution characteristics of the landslide, we suggested that the epicenter of the Qishan earthquake may be located in northwestern Qishan, near Fengxiang, with a possible magnitude of Mw7.3 (M7.6) and possible seismogenic structure belonging to the Longxian–Qishan–Mazhao Fault along the Longxian–Qishan segment.

We note that if landslides in a target area can be confirmed to have been triggered by a single strong historical earthquake, a "relatively complete" coseismic landslide database of historical earthquakes can be obtained using current high-resolution satellite images. This could provide more objective evidence for the revision of source parameters associated with strong historical earthquakes as compared with the use of historical records.

DATA AVAILABILITY STATEMENT

The original contributions presented in the study are included in the article/Supplementary Material, further inquiries can be directed to the corresponding author.

AUTHOR CONTRIBUTIONS

XY proposed and participated in designing the study; DP designed the study, analyzed the data and wrote the manuscript; TQ participated in designing the study and improved the paper; LW participated in designing the study; All authors approved the final version of the manuscript.

FUNDING

The authors would like to extend their thanks to the National Natural Science Foundation of China (No. 42072248), the National Key Research and Development Program (No. 2019YFE0108900), the Seismic Active Fault Exploration Project based on High-Resolution Remote Sensing Interpretation Technology by the Department of Earthquake Damage Defense, CEA (No. 15230003), and the China Scholarship Council (No. 201604190021).

REFERENCES

Chen, X., Hui, H., and Zhao, Y. (2014). Study on the fault mechanics influences on the landslides distribution: a case study from the Wenchuan earthquake. *Seismol. Geol.* 36, 358–367. doi:10.3969/j.issn.0253-4967.2014.02.007 (in Chinese).

Cheng, J., Rong, Y., Magistrale, H., and Chen, G. (2017). An mw-based historical earthquake catalog for mainland China: an MW-based historical earthquake catalog for mainland China. *Bull. Seismol. Soc. Am.* 107, 2490–2500. doi:10.1785/0120170102

Dadson, S., Hovius, N., Chen, H., Dade, W., Lin, J., and Hsu, M. (2004). Earthquake-triggered increase in sediment delivery from an active mountain belt. *Geology* 32, 733–736. doi:10.1130/G20639.1

Deng, Q. (2011). *The Climatic evolution during the Holoeene in the Bao ji region.* Xi'an: Chang'an University, 1–64. (in Chinese).

Department of Earthquake Disaster Prevention National Earthquake Administration. (1995). *Catalog of historical strong earthquakes in China.* Beijing: Earthquake Press, 1–514. (in Chinese).

Du, F., Wen, X., Feng, J., Liang, M., Long, F., and Wu, J. (2018). Seismo-tectonics and seismic potential of the Liupanshan fault zone (LPSFZ), China. *Chin. J. Geophys.* 61, 545–559. doi:10.6038/cjg2018L0181 (in Chinese).

Du, P., Xu, Y., Tian, Q., Zhang, W., and Liu, S. (2020a). The spatial distribution and attribute parameter statistics of landslides triggered by the may 12th, 2008, Mw7.9 wenchuan earthquake. *Earthq. Res. China* 34, 29–49.

Du, P., Xu, Y., Li, W., Tian, Q., and Chen, L. (2020b). Volume calculation of landslides and dammed lake sediments triggered by a strong historical earthquake on the loess plateau: a case study of Qiuzigou, gansu province, northwest China. *Earthq. Res. China.*, 34, 54–59. (in press).

Gu, G. (1983). *Catalog of earthquakes in China (1831–1969 BC).* Beijing: Science Press. (in Chinese).

Lanzhou Institute of Earthquake Research, National Seismological Administration (1985). *Catalog of strong earthquakes in the four provinces (regions) of Shaanxi, Gansu, Ningxia and Qinghai.* Xi'an: Shaanxi Science and Technology Press. (in Chinese).

Larsen, I., Montgomery, D., and Korup, O. (2010). Landslide erosion controlled by hillslope material. *Nat. Geosci.* 3, 247–251. doi:10.1038/ngeo776

Li, C. (2019). The Relationship between strain accumulation characteristics and seismic moment release on the southwestern margin of Ordos block. (in Chinese)

Li, S. (1960). *Catalog of earthquakes in China.* Beijing: Seismological Press. (in Chinese).

Li, W., Huang, R., Pei, X., and Zhang, X. (2015). Historical co-seismic landslides inventory and analysis using Google Earth: a case study of 1920 M8.5 Haiyuan earthquake, China. *Eng. Geol. Soc. Territ.*, 2. Switzerland: Springer, 709–712.

Li, X. (2018). Deformation pattern based on geometry and kinematics of active tectonics in the southwestern Ordos block. *Recent Dev. World Seismol.* 5, 43–45. doi:10.3969/j.issn.0253-4975.2018.05.009 (in Chinese).

Li, X., Feng, X., Li, X., Li, C., Zheng, W., Zhang, P., et al. (2019). Geological and geomorphological evidence for active faulting of the southern Liupanshan fault zone, NE Tibetan plateau. *Geomorphology* 345, 1–11. doi:10.1016/j.geomorph.2019.106849

Li, Z., Yang, L., Wang, G., Hou, J., Xin, Z., Liu, G., et al. (2019). Current status, problems and countermeasures of soil erosion control in the Loess Plateau. *Acta Ecol. Sin.* 39, 7398–7409. doi:10.5846/stxb201909021821 (in Chinese).

Meunier, P., Hovius, N., and Haines, J. (2008). Topographic site effects and the location of earthquake induced landslides. *Earth Planet Sci. Lett.* 275, 221–232. doi:10.1016/j.epsl.2008.07.020

National Earthquake Administration. (1988). *Ordos peripheral active fault system.* Beijing: Seismological Press. (in Chinese).

Parker, R., Densmore, A., Rosser, N., De, M., Li, Y., Huang, R., et al. (2011). Mass wasting triggered by the 2008 Wenchuan earthquake is greater than orogenic growth. *Nat. Geosci.* 4, 449–452. doi:10.1038/ngeo1154

Peng, J. (1992). Structural evolution and seismicity of the Weihe fault zone. *Seismol. Geol.* 14, 113–120. (in Chinese).

Ran, H. (2011). Empirical relations between earthquake magnitude and parameters of strike-slip seismogenic active faults associated with historical earthquakes in western China. *Seismol. Geol.* 33, 577–585. doi:10.3969/j.issn.0253-4967.2011.03.008 (in Chinese).

Song, F., Yuan, D., Chen, G., Ge, W., Cheng, J., and Su, H. (2007). Pattern and combination features of the surface ruptures of the 1125 A.D. Lanzhou M7 earthquake. *Seismol. Geol.* 29, 834–844. doi:10.3969/j.issn.0253-4967.2007.04.014 (in Chinese).

Sun, P., LiJiang, R. h., Lgwe, O., and Shi, J. (2017). Earthquake-triggered landslides by the 1718 Tongwei earthquake in gansu province, northwest China. *Bull. Eng. Geol. Environ.* 76, 1281–1295. doi:10.1007/s10064-016-0949-4

Sun, Y., Xu, G., Long, H., and Xu, L. (2016). Relationship between magnitude and rupture length. *Acta Seismol. Sin. (Chin. Ed.).* 38 (5), 803–806. doi:10.11939/jass.2016.05.014

Wang, A., Yuan, D., and Lei, Z. (2018). The distribution characteristics of seismic hazard and seismogenic structure of the southern Tianshui M6.0 Earthquake in 1936. *Earthq. Res. China* 34, 788–799. doi:10.3969/j.issn.1001-4683.2018.04.019 (in Chinese).

Wang, L. M. (2003). *Loess dynamics.* Beijing: Seismological Press. (in Chinese).

Wang, S. (2018). *Late Cenozoic structural deformation characteristics of the Liupanshan–Baoji fault zone on the northeastern margin of the Qinghai–Tibet Plateau.* Kirkland: Northwest University. (in Chinese).

Wells, D., and Coppersmith, K. (1994). Empirical relationships among magnitude, rupture length, rupture area, and surface displacement. *Bull. Seismol. Soc. Am.* 84, 974–1002. doi:10.1007/BF00808290

Xu, C., Xu, X., Yao, X., and Dai, F. (2014). Three (nearly) complete inventories of landslides triggered by the May 12, 2008 Wenchuan Mw 7.9 earthquake of China and their spatial distribution statistical analysis. *Landslides* 11, 441–461. doi:10.1007/s10346-013-0404-6

Xu, C., Xu, X., Zheng, W., Min, W., Ren, Z., and Li, Z. (2013). Landslides triggered by the 2013 Minxian-Zhangxian, Gansu province Ms6.6 earthquake and its tectonic analyses. *Seismol. Geol.* 35, 616–626. doi:10.3969/j.issn.0253-4967.2013.03.015 (in Chinese).

Xu, Y., Allen, M., Zhang, W., Li, W., and He, H. (2020a). Landslide characteristics in the loess plateau, northern China. *Geomorphology* 359, 107150. doi:10.1016/j.geomorph.2020.107150

Xu, Y., Du, P., Li, W., Zhang, W., Tian, Q., Xiong, R., et al. (2020b). A case study on AD 1718 Tongwei M7.5 earthquake triggered landslides—application of landslide database triggered by historical strong earthquakes on the Loess Plateau. *Chin. J. Geophys.* 63, 1235–1248. doi:10.6038/cjg2020N0146

Xu, Y., Liu-Zeng, J., Allen, M., Zhang, W., and Du, P. (2020c). Landslides of the 1920 Haiyuan earthquake, northern China. *Landslides* doi:10.1007/s10346-020-01512-5

Xu, Y., Zhang, W., Li, W., He, H., and Tian, Q. (2018). Distribution characteristics of the ad 1556 Huaxian earthquake triggered disasters and its implications. *Seismol. Geol.* 40, 721–737. doi:10.3969/j.issn.0253-4967.2018.04.001

Yang, X., Feng, X., Huang, X., Song, F., Li, G., Chen, X., et al. (2015). The Late Quaternary activity characteristics of the Lixian-Luojiabu fault: a discussion on the seismogenic mechanism of the Lixian M8 earthquake in 1654. *Chin. J. Geophys.* 58, 504–519. doi:10.6O38/cjg2O15O214

Ye, M., Meng, G., and Su, X. (2018). Locking characteristics and slip deficits of the main faults in the northeast margin of Tibetan plateau. *Earthquake* 38, 1–12. doi:10.3969/j.issn.1000-3274.2018.03.001

Yuan, D., Ge, W., Chen, Z., Li, C., Wang, Z., Zhang, H., et al. (2013). The growth of northeastern Tibet and its relevance to large-scale continental geodynamics: a review of recent studies. *Tectonics* 32, 1358–1370. doi:10.1002/tect.20081

Yuan, D., Lei, Z., and Wang, A. (2017). Additional textual criticism of southern Tianshui M8 earthquake in gansu province in 1654. *China Earthq. Eng. J.* 39, 0509–0520. 10.1155/2012/461863

Yuan, R., Deng, Q., Cunningham, D., Xu, C., Xu, X., and Chang, C. (2013). Density distribution of landslides triggered by the 2008 Wenchuan earthquake and their relationships to peak ground acceleration. *Bull. Seismol. Soc. Am.* 103, 2344–2355. doi:10.1785/0120110233

Zhang, B., He, W., Fang, L., Pang, W., Zhao, Z., and Liu, X. (2015). Surveys on surface ruptures phenomena of gansu kangle M6 3/4 earthquake in 1936. *J. Seismol. Res.* 38, 262–271. doi:10.3788/gzxb20184703.0324003

Zheng, D., Wang, W., Wan, J., Yuan, D., Liu, C., Zheng, W., et al. (2017). Progressive northward growth of the northern qilian Shan–hexi corridor (northeastern tibet) during the cenozoic. *Lithosphere* 9, 5877–5891. doi:10.1130/L587.1

Zheng, W., Lei, Z., Yuan, D., He, W., Ge, W., and Liu, X. (2007). Structural research on the 1837 northern Minxian M6 earthquake in Gansu Province and its causative structure. *Earthquake* 27, 120–130. doi:10.3969/j.issn.1000-3274.2007.01.016

Zheng, W., Zhang, P., He, W., Yuan, D., Shao, Y., Zheng, D., et al. (2013). Transformation of displacement between strike-slip and crustal shortening in the northern margin of the Tibetan Plateau: evidence from decadal GPS measurements and late Quaternary slip rates on faults. *Tectonophysics* 584, 267–280. doi:10.1016/j.tecto.2012.01.006

Conflict of Interest: The authors declare that the research was conducted in the absence of any commercial or financial relationships that could be construed as a potential conflict of interest.